Received: 17 November 2021 | Revised: 25 March 2022 | Accepted: 29 April 2022 | Published on: 15 May 2022

DOI: 10.1002/joc.7689

International Journal of Climatology RMetS

RESEARCH ARTICLE

Spatiotemporal variations of extreme events in surface mass balance over Greenland during 1958–2019

Ting Wei[1] | **Brice Noël**[2] | **Minghu Ding**[1] | **Qing Yan**[3,4]

[1]State Key Laboratory of Severe Weather, Chinese Academy of Meteorological Sciences, Beijing, China

[2]Institute for Marine and Atmospheric Research (IMAU), Utrecht University, Utrecht, the Netherlands

[3]Nansen-Zhu International Research Centre, Institute of Atmospheric Physics, Chinese Academy of Sciences, Beijing, China

[4]Key Laboratory of Meteorological Disaster/Collaborative Innovation Center on Forecast and Evaluation of Meteorological Disasters, Nanjing University of Information Science and Technology, Nanjing, China

Correspondence
Ting Wei, Chinese Academy of Meteorological Sciences, Beijing 100081, China.
Email: weiting@cma.gov.cn

Funding information
National Natural Science Foundation of China, Grant/Award Number: 41975120; NWO VENI, Grant/Award Number: VI. Veni.192.019; Strategic Priority Research Program of the Chinese Academy of Sciences, Grant/Award Number: XDA2010030807

Abstract

Greenland surface mass balance (SMB) is undergoing dramatic change due to the amplified Arctic warming, with more frequent record-breaking melt events. To comprehensively understand the behaviour of the Greenland ice sheet, we develop a suite of indices to examine the spatiotemporal variations of extreme events in SMB over Greenland during 1958–2019 based on the RACMO2.3p2 model outputs. We illustrate that the climatological distributions of extreme ablation-dominated events (i.e., extremes with SMB < 0) share large similarity with the mean SMB in terms of intensity and frequency, showing a coastal-to-inland decreasing pattern. This pattern holds for the intensity of the extreme accumulation-dominated events (i.e., extremes with SMB > 0), but not for the frequency which increases from the coastal to inland Greenland. Regarding the temporal evolution, the intensity and frequency of extreme ablation-dominated events show a decreasing trend over Greenland during 1958–1978, whereas the trend increases afterwards, especially during the last two decades (2001–2019). However, these trends fluctuate regionally across the GrIS both in terms of magnitude and sign, with the most pronounced variations occurring in southwest Greenland. In contrast, extreme accumulation-dominated events show, on average, a long-term increasing trend from 1958 to 2019 in terms of intensity and frequency. However, obvious spatial fluctuations exist across the GrIS during 1958–2019, especially between the southwest and northeast Greenland where an opposite trend is observed. Additionally, the variations of SMB extremes in boreal summer are linked with the changes in regional temperature and precipitation and the associated atmospheric circulations, and the dominating factor varies with different extreme indices and time intervals. Our results may advance our understanding on SMB variability over Greenland and contribute to the design of future Greenland observational networks.

KEYWORDS

ablation, accumulation, extreme indices, RACMO2.3p2 model, spatial distribution, temporal trend

1 | INTRODUCTION

The Arctic is warming three times faster than the global average from 1971 to 2019 (AMAP, 2021). The warmer Arctic strongly impacts its environment and could induce global climatic influences via teleconnection (Thompson and Wallace, 1998; Serreze and Barry, 2011; Cohen *et al.*, 2014). One of the most pronounced environmental manifestations of Arctic warming is the accelerated melting of the Greenland ice sheet (GrIS; Noël *et al.*, 2019). Over the last 27 years (1992–2018), mass loss from the GrIS raised global mean sea level by 10.8 ± 0.9 mm (The IMBIE Team, 2020), contributing ~20% to the observed global sea-level rise (Frederikse *et al.*, 2020). Variation of surface mass balance (SMB), defined as snowfall accumulation and ablation from meltwater runoff and sublimation, primarily contributes to ongoing GrIS mass loss (Van den Broeke *et al.*, 2017; Mouginot *et al.*, 2019). According to the estimated SMB from three regional climate models, a decrease in SMB leads to ~2,000 Gt of ice loss between 1992 and 2018, contributing over half (50.3%) of total GrIS mass loss (The IMBIE Team, 2020). The reduced SMB in recent decades results largely from increased meltwater runoff and is tied to warmer atmospheric conditions. Notably, the contribution of SMB to GrIS mass loss varies largely with time, for example, accounting for 70% of all mass losses from 2007 to 2012 (The IMBIE Team, 2020). Moreover, the decreased SMB could amplify the surface warming and foster further melting via the positive surface melt–albedo and SMB–elevation feedbacks (Box *et al.*, 2012; Edwards *et al.*, 2014; Ryan *et al.*, 2019).

On top of a continuous SMB decline, a succession of extreme surface melt events has been observed over Greenland during the past decades. A record-breaking melt event was observed in July 2012, with surface melt extending over nearly the entire GrIS. This extreme melt event is linked with the anomalous blocking high pressure and negative North Atlantic Oscillation that favours southerly warm air advection (Nghiem *et al.*, 2012; Hanna *et al.*, 2014). During the warm summer of 2019, the GrIS experienced an exceptional mass loss of 600 Gt, resulting in the largest annual ice loss on record since 1948 (Tedesco and Fettweis, 2020). Besides, there is an increase in extreme climate/weather events over the Arctic in terms of frequency and magnitude during recent decades (Graham *et al.*, 2017), which are potentially favourable for surface melting (Niwano *et al.*, 2021). For example, an extreme rainfall event occurred at the summit of the Greenland during 2021 summer, which has not been reported before and is associated with widespread surface melting (https://nsidc.org/greenland-today/2021/08/rain-at-the-summit-of-greenland/).

As Earth's climate continues to warm, extreme melt events may become more pronounced and frequent over Greenland. The occurrence of extreme melt events could not only accelerate the mass loss of the GrIS but also has significant global climatic influences owing to the associated meltwater inputs, for example, leading to substantial slowing of the Atlantic overturning circulation (Liu *et al.*, 2018; Golledge *et al.*, 2019). Thus, a better understanding of current changes in SMB-related extreme events may advance our knowledge of the behaviour of the GrIS. However, a systematic assessment of extreme SMB events during the recent decades has not yet been addressed. This comes about due to the lack of (a) a high-quality continuous daily dataset covering the entire GrIS that is essential for extreme events analysis and (b) definitions for extreme SMB events that could be easily applied and compared to other extreme climate indices. Alternatively, it is important to utilize model simulations to provide a scenario on the spatiotemporal variations of SMB extremes. Recently, the Arctic climate simulations by Regional Atmospheric Climate Model (RACMO2.3p2), a state-of-the-art regional climate model that is specifically adapted to simulate polar climates, provide reliable results for the GrIS SMB compared with in situ observations (Noël *et al.*, 2018; Van Dalum *et al.*, 2021).

In this study, we attempt to develop a series of metrics for SMB extremes in the hope that they could be easily calculated and applied for both observations and model results. Then we provide the first evaluation of the extreme events in SMB over Greenland based on the RACMO2.3p2 simulations. The estimates of SMB extremes over Greenland may contribute to identify extreme events for other Arctic glaciers, to decipher recent changes in SMB, and to better project the future evolution of the GrIS.

2 | DATA AND METHODS

2.1 | Datasets

The daily SMB over Greenland is obtained from the regional climate model RACMO2.3p2, which is specifically developed for use over glaciated regions. It is suggested that the RACMO2.3p2 has the most accurate representation of SMB over the GrIS accumulation and ablation zones compared with available observations (Fettweis *et al.*, 2020). The model is run at a horizontal resolution of 5.5 × 5.5 km and is forced by a combination of reanalysis datasets from the ERA40 (1958–1978), ERA-Interim (1979–1989), and the ERA5 (1990–2019) (Noël *et al.*, 2019). Additionally, we use the ERA5 atmospheric

TABLE 1 Indices for extreme events in SMB

Index	Description	Formula	Interpretation
BX	The strongest ablation-dominated daily events	The minimum value of negative daily SMB	SMB amount (unit: mm·w.e.·day^{-1})
AX	The strongest accumulation-dominated daily events	The maximum value of positive daily SMB	
BD95n	Extreme ablation-dominated days	The number of days with SMB < B95 in 1 year. B95 is the 95th percentile of SMB for negative SMB days (on basis of 1986–2005, consistent with the reference period in IPCC-AR6)	Day count; percentile threshold (unit: days)
AD95n	Extreme accumulation-dominated days	The number of days with SMB > A95 in 1 year. A95 is the 95th percentile of SMB for positive SMB days (on basis of 1986–2005)	
BD95p	Fraction due to BD95n	The ratio of SMB during BD95n days to total amount of negative SMB: $\mathrm{BD95p}=\frac{\sum \text{SMB where SMB<B95}}{\sum \text{SMB where SMB<0}}$.	Fraction; percentile threshold (unit: %)
AD95p	Fraction due to AD95n	The ratio of SMB during AD95n days to total amount of positive SMB: $\mathrm{AD95p}=\frac{\sum \text{SMB where SMB>A95}}{\sum \text{SMB where SMB>0}}$	

reanalysis at 0.25° × 0.25° resolution to investigate large-scale atmospheric circulation patterns associated with changes in extreme SMB events.

2.2 | Extreme indices

A total of six extreme indices (Table 1) are proposed here for the first time to estimate the intensity and frequency of extreme SMB events over Greenland based on daily model outputs. We divide extreme SMB events into two categories: extreme negative events (SMB < 0; hereafter referred to ablation-dominated events) and extreme positive events (SMB > 0; hereafter referred to accumulation-dominated events). Specifically, we use the number of days with the amount of negative/positive SMB above the 95th percentile (BD95n/AD95n) to measure the frequency of extreme daily ablation/accumulation-dominated events. The minimum value of negative daily SMB (BX) is adopted as indicator for the intensity of ablation-dominated events, and the maximum value of positive daily SMB (AX) is used for accumulation-dominated events. Additionally, we employ the ratio of SMB amount during BD95n/AD95n days to the total SMB amount (AD95p/BD95p) to represent the intensity of ablation/accumulation-dominated events. BD95p/AD95p and BX/AX are relative and absolute indicators for extreme SMB events, respectively. These indicators (BX vs. BD95p and AX vs. AD95p) depicts different aspects of the SMB intensity and hence provide more comprehensive information for understanding extreme events over Greenland. In addition, the annual ablation/accumulation (BA/AA), defined as the annual mean of negative/positive daily SMB, indicates the mean state of daily ablation/accumulation-dominated SMB over the GrIS.

3 | RESULTS

We first briefly examine the variation of annual mean SMB over Greenland for the period of 1958–2019, which provides a general background for extreme events. Annual mean SMB averaged over GrIS exhibits obvious interannual and interdecadal fluctuations during 1958–2019. A clear interdecadal shift in the linear trend of SMB is observed around the late-1970s, with an increasing trend before late-1970s and a declining trend afterwards (Figure 1a). Moreover, there is a significant interdecadal shift in annual mean SMB around 2000 according to the Mann–Kendall test (Figure 1b), indicating a recent phase of relatively lower and more rapid loss of the GrIS SMB than that before 2000. Therefore, we divide the entire period (1958–2019) into three subperiods, with the first interval covering the period of 1958–1978 (P1), the second one from 1979 to 2000 (P2), and the third interval between 2001 and 2019 (P3). Note that the selection of the three subperiods may be influenced by the nonhomogeneity of climatic forcings, which are derived from ERA40 over 1958–1978, ERA-Interim over 1979–1989 and ERA5 over 1990–2019. But the modelled

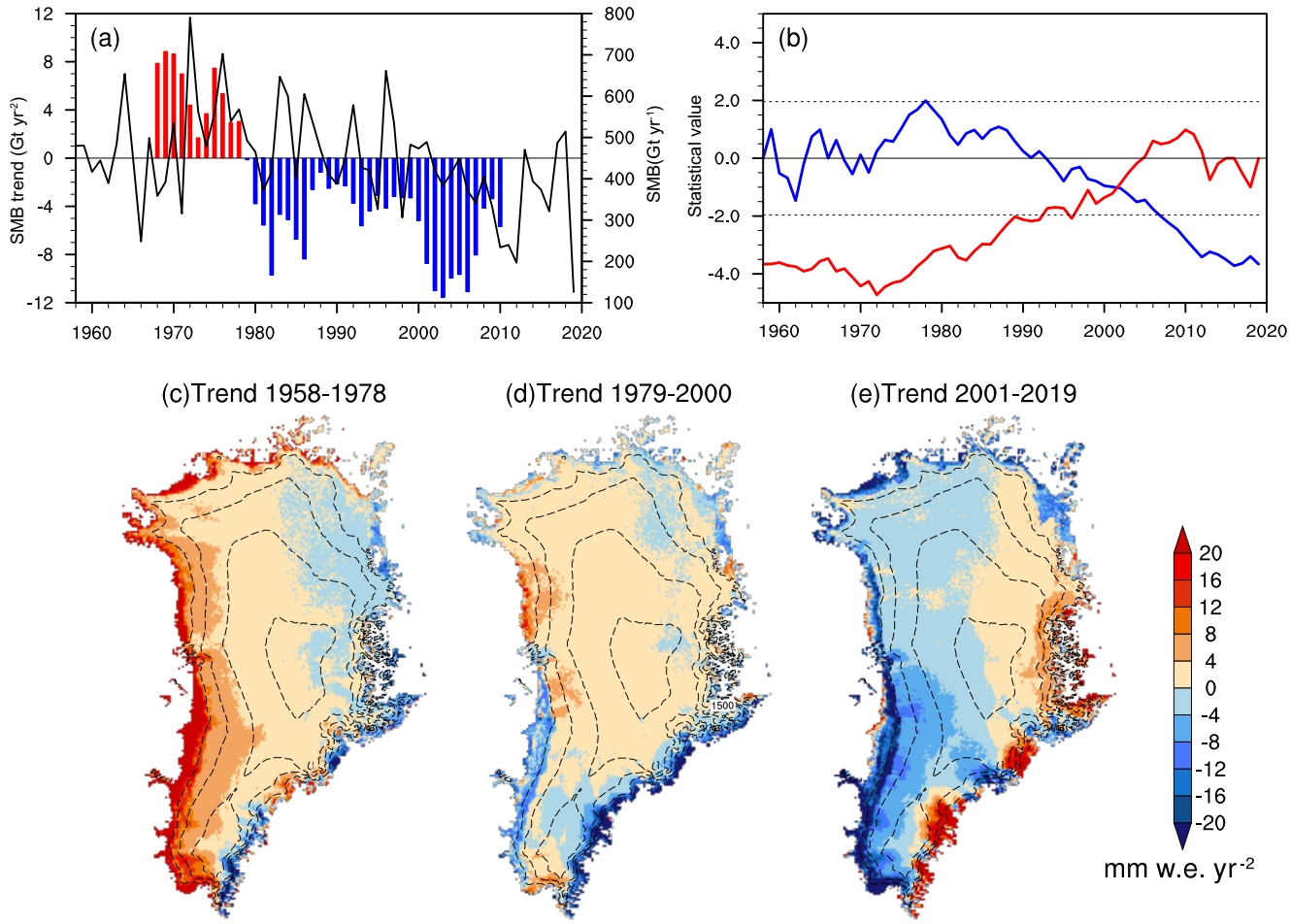

FIGURE 1 (a) The time series of the GrIS SMB averaged over the GrIS (Gt·year^{-1}; black line) and its 10-year running trend (Gt·year^{-2}; colour bars). (b) Mann–Kendall test for the SMB averaged over the GrIS. In the Mann–Kendall abrupt test, UF (UB) is a sequence of statistics calculated according to (in reverse order of) the time series of SMB, which is shown in blue (red) line. The blue/red line refers to the curve of UF/UB. The dashed lines refer to the critical lines that indicate statistical significance at the 95% level. When UF and UB curves intersect and the intersection is between the critical line, the time of intersection point is the beginning of abrupt change. (c–e) The distribution of the trend in annual mean SMB (unit: mm·w.e.·year^{-2}) during the (c) P1, (d) P2, and (e) P3 periods [Colour figure can be viewed at wileyonlinelibrary.com]

mean SMB from the RACMO2.3p2 simulations used here has been validated by observational data in previous studies (e.g., Fettweis *et al.*, 2020; Slater *et al.*, 2021; van Dalum *et al.*, 2021).

Notably, there are obvious differences in the spatial pattern of SMB trend across the GrIS during the three subperiods (Figure 1c–e). SMB shows a significant increasing trend over the majority of the GrIS before 1978, especially over the western marginal regions, though an insignificant decreasing trend is broadly seen along the eastern coasts of Greenland. In contrast, the trend of the regionally averaged SMB turns to be negative during 1979–2000, with the largest contribution from the southeast GrIS. After 2000, the western and northern GrIS experiences remarkable reduction in SMB, resulting in an overall decreasing trend over the GrIS, while SMB broadly shows an insignificant increasing trend over the low-lying eastern GrIS. The spatial pattern of SMB trend during the P3 period is generally opposite to that during the P1 period. Next, we investigate the spatiotemporal variations of extreme events in SMB in the following subsections.

3.1 | Extreme ablation-dominated events

3.1.1 | Intensity

Figure 2a shows the climatological distribution for annual BX over the GrIS during 1958–2019. The absolute

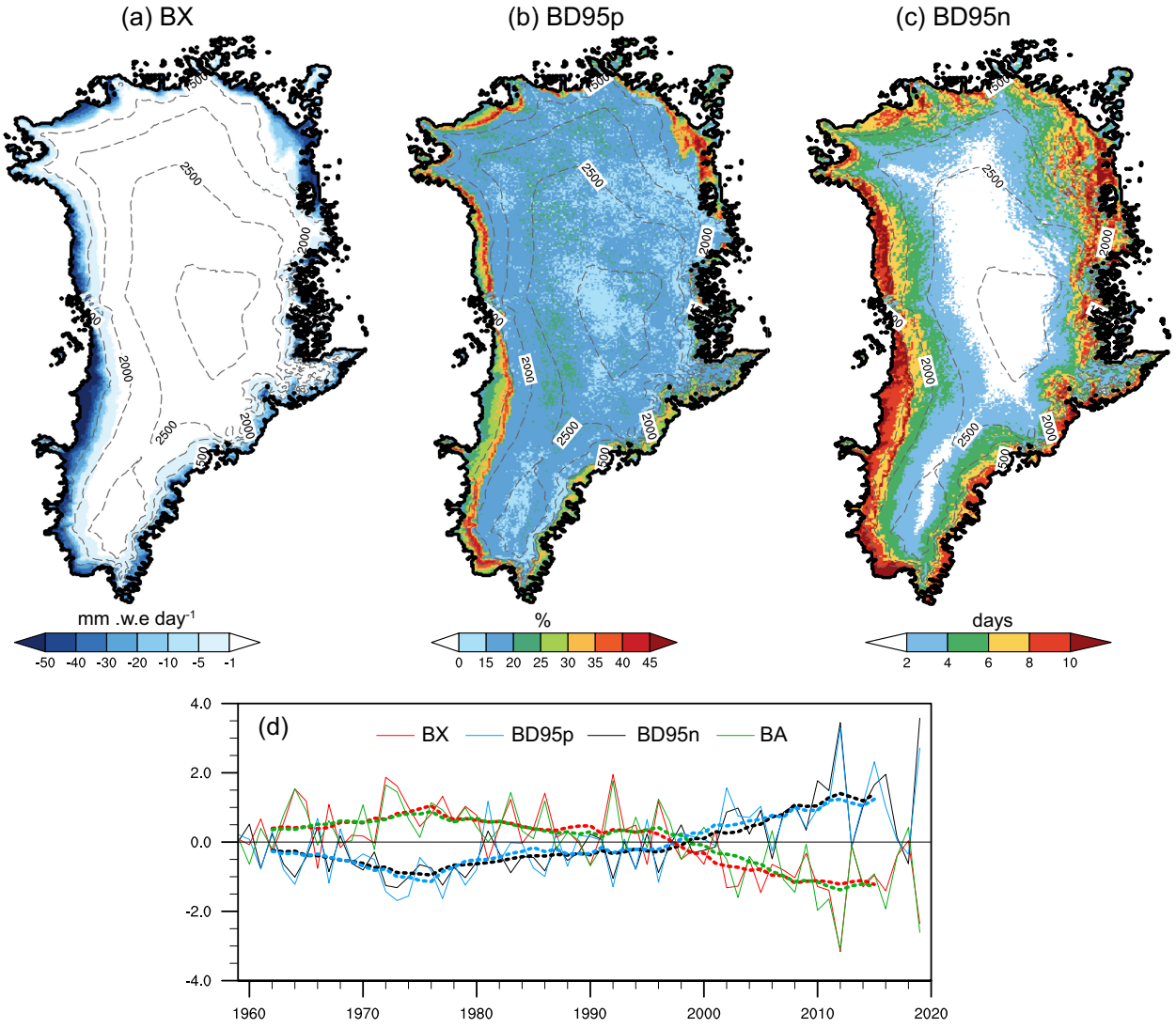

FIGURE 2 Climatological distributions of (a) BX, (b) BD95p, and (c) BD95n over the GrIS during 1958–2019. (d) The standardized time series of BX, BD95p, BD95n and BA averaged over the GrIS (solid lines) from 1958 to 2019 and its 9-year running mean (dotted lines). Note that BX and BA themselves are negative [Colour figure can be viewed at wileyonlinelibrary.com]

value of annual BX shows a decreasing pattern from the coastal to inland areas and reduces to almost zero above ~1,500 m (which also represents the average equilibrium line altitude where SMB = 0) over Greenland. The relatively stronger ablation-dominated events (<−30 mm·w.e.·day^{-1}) is mainly observed over the southwest GrIS, where most glaciers are land terminating and the mean ablation is the largest (van den Broeke *et al.*, 2009). The coastal-to-inland decreasing pattern also holds for the BD95p (another metric for the intensity of extreme ablation-dominated events), which spans from ~25% to 45% for elevations below ~1,500 m and is below 15% in the interior of the GrIS (Figure 2b). Regarding the temporal evolution, during the past six decades, the intensity of extreme ablation-dominated events, as measured by BX (itself is negative), on average experiences a remarkable weakening trend before 1978 but a strengthening trend afterwards, especially after 2000 (Figure 2d). This temporal pattern is generally confirmed by the variation of the BD95p. The evolution of annual mean ablation (i.e., BA) and BD95p shares large similarity with BX in terms of interannual variation and long-term trend, but with different changing rates (e.g., Figure 3).

Furthermore, we investigate the spatial patterns of the trends in BX across the GrIS during the three subperiods (Figure 3). The annual BX shows an upward trend over the GrIS from 1958 to 1978, especially over the north and southwest GrIS where the trend reaches 0.08 and 0.15 mm·w.e.·day^{-1}·year^{-1} (passing the 90% level of significance test), respectively. This indicates a significantly reduced intensity of extreme ablation-dominated events over the two regions during 1958–1978, as BX itself is

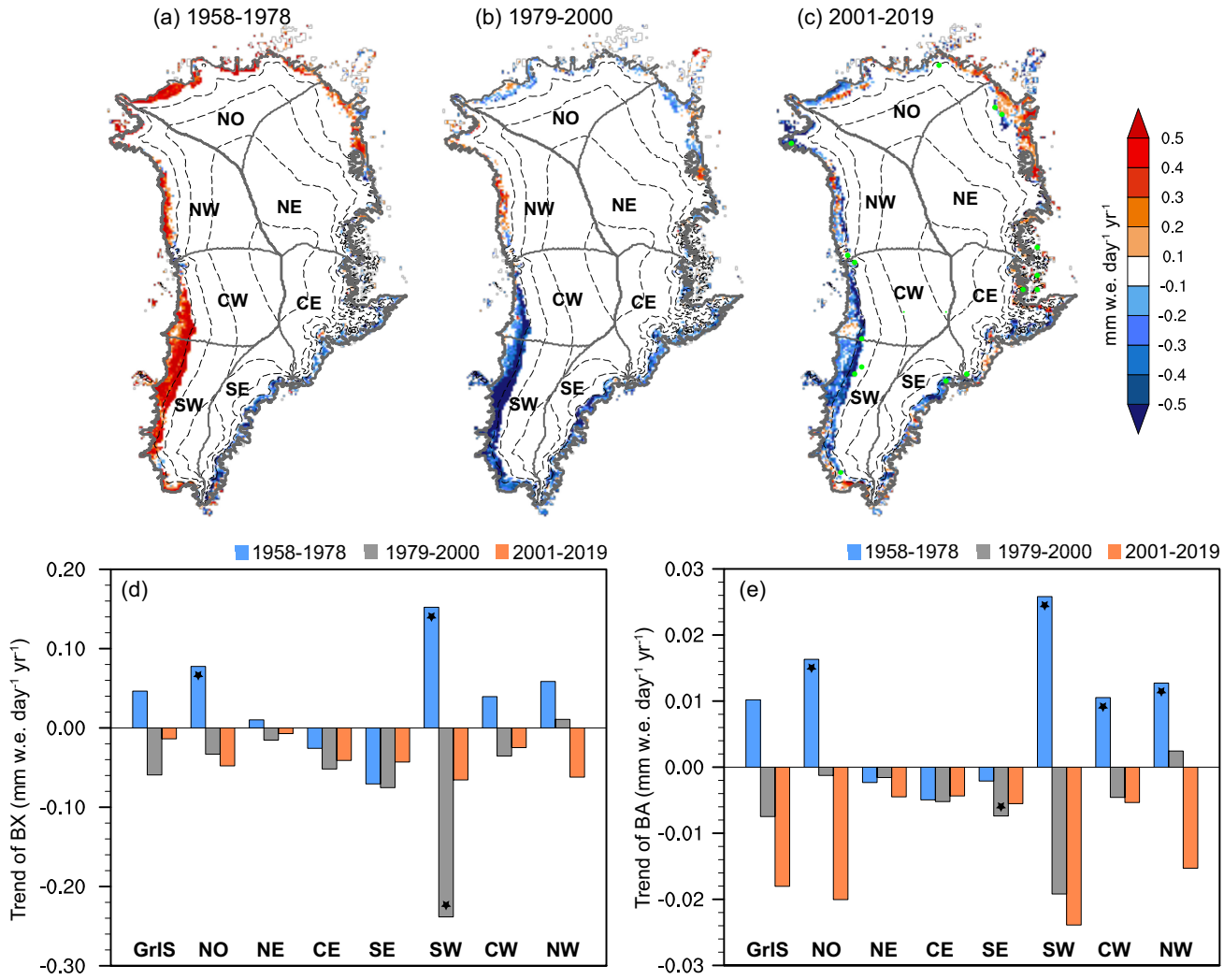

FIGURE 3 (a–c) The distribution of annual BX trend during (a) P1 (1958–1978), (b) P2 (1979–2000), and (c) P3 (2001–2019) periods. The GrIS is divided into seven regions based on Mouginot *et al.* (2019): (i) southwest (SW), (ii) central west (CW), (iii) northwest (NW), (iv) north (NO), (v) northeast (NE), (vi) central east (CE), and (vii) southeast (SE) GrIS. Regionally averaged trend in (d) BX and (e) BA during the three subperiods. The trend that is statistically significant at 90% level is marked with green dots and stars [Colour figure can be viewed at wileyonlinelibrary.com]

negative. However, an insignificant downward trend in BX is seen over the central-east and southeast GrIS at that time. During 1979–2000, the intensity of extreme ablation-dominated events becomes stronger almost over the entire Greenland, manifested by a descending trend in BX. However, the declining trend passes the statistical significance test only over the southwest GrIS (-0.24 mm·w.e.·day^{-1}·year^{-1}). The intensity of extreme ablation-dominated events is further intensified over the entire GrIS after 2000, though with an insignificant decreasing trend. Although BX and BA have similar trends across individual regions of the GrIS during the three subperiods, the magnitude of the trend in BX is generally larger than that in BA. For example, BA shares the similar significant upward trend with BX over the north and southwest GrIS where the trend is 0.016 and 0.026 mm·w.e.·day^{-1}·year^{-1} from 1958 to 1978.

The spatiotemporal evolution of BD95p shares large similarity with the BX (Figure 4). Specifically, the BD95p tends to decrease over the GrIS during 1958–1978, especially over the western (from -0.42 to -0.45%·year^{-1}) and northern (-0.49%·year^{-1}) parts of the GrIS, suggesting reduced intensity of extreme ablation-dominated events over these regions. In contrast, the BD95p shows an increasing trend during the P2 and P3 periods over the majority of the GrIS (0.36–0.45%·year^{-1}), with more profound changes over the central-west and southern parts of Greenland.

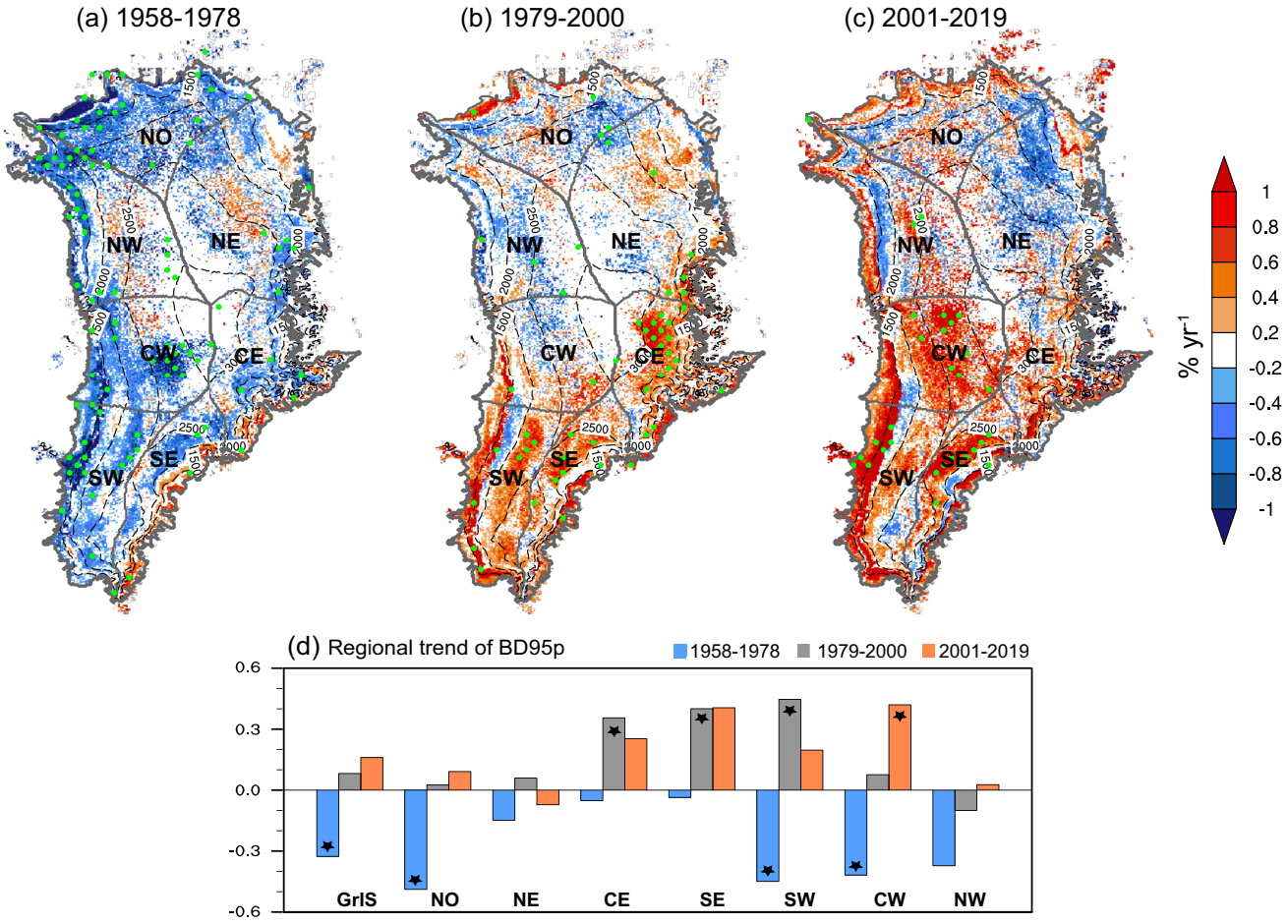

FIGURE 4 (a–c) The distribution of annual BD95p trend during (a) P1 (1958–1978), (b) P2 (1979–2000), and (c) P3 (2001–2019) periods. (d) Regionally averaged trend in BD95p during the three subperiods. The trend that is statistically significant at 90% level is marked with green dots and stars [Colour figure can be viewed at wileyonlinelibrary.com]

Overall, the two indices measuring the intensity of extreme ablation-dominated events show similar trend in terms of temporal evolution and spatial pattern, highlighting a robust change in the ablation-dominated extreme events.

3.1.2 | Frequency

According to the BD95n, the frequency of extreme ablation-dominated events shows a decreasing pattern from the coastal to inland areas in terms of climatological distribution (Figure 2c). The BD95n averaged over the low-lying regions is approximately 8 days, with the maximum value of >12 days. This decreases to 0–2 days over the interior of the GrIS. For the temporal evolution, there is a decreasing trend with large interannual fluctuations in BD95n averaged over the GrIS during 1958–1978, indicating decreased frequency of extreme ablation-dominated events. This is followed by a long-term increasing trend afterwards, that is, more frequent extreme ablation-dominated events during 1979–2019 (Figure 2d).

Regarding the spatial pattern in temporal trend, annual BD95n shows a significant decreasing trend (−0.1 days·year^{-1}) from 1958 to 1978. The decreasing trend is observed over the entire GrIS, with more profound changes (−0.11 to −0.14 days·year^{-1}) over the western parts. During the period 1979–2000, there is a significant increasing trend in the extreme ablation-dominated days over the central-east and southeast GrIS, where the trend is 0.12 and 0.18 days·year^{-1}, respectively. In the meantime, BD95n tends to vary in an opposite fashion between the southwest and the northwest GrIS, though with an insignificant trend. From 2001 to 2019, the extreme ablation-dominated events occur more frequently almost over the entire Greenland compared with the earlier period. The most significant change in BD95n is found in central-west GrIS, with an increasing trend of 0.22 days·year^{-1} (Figure 5)

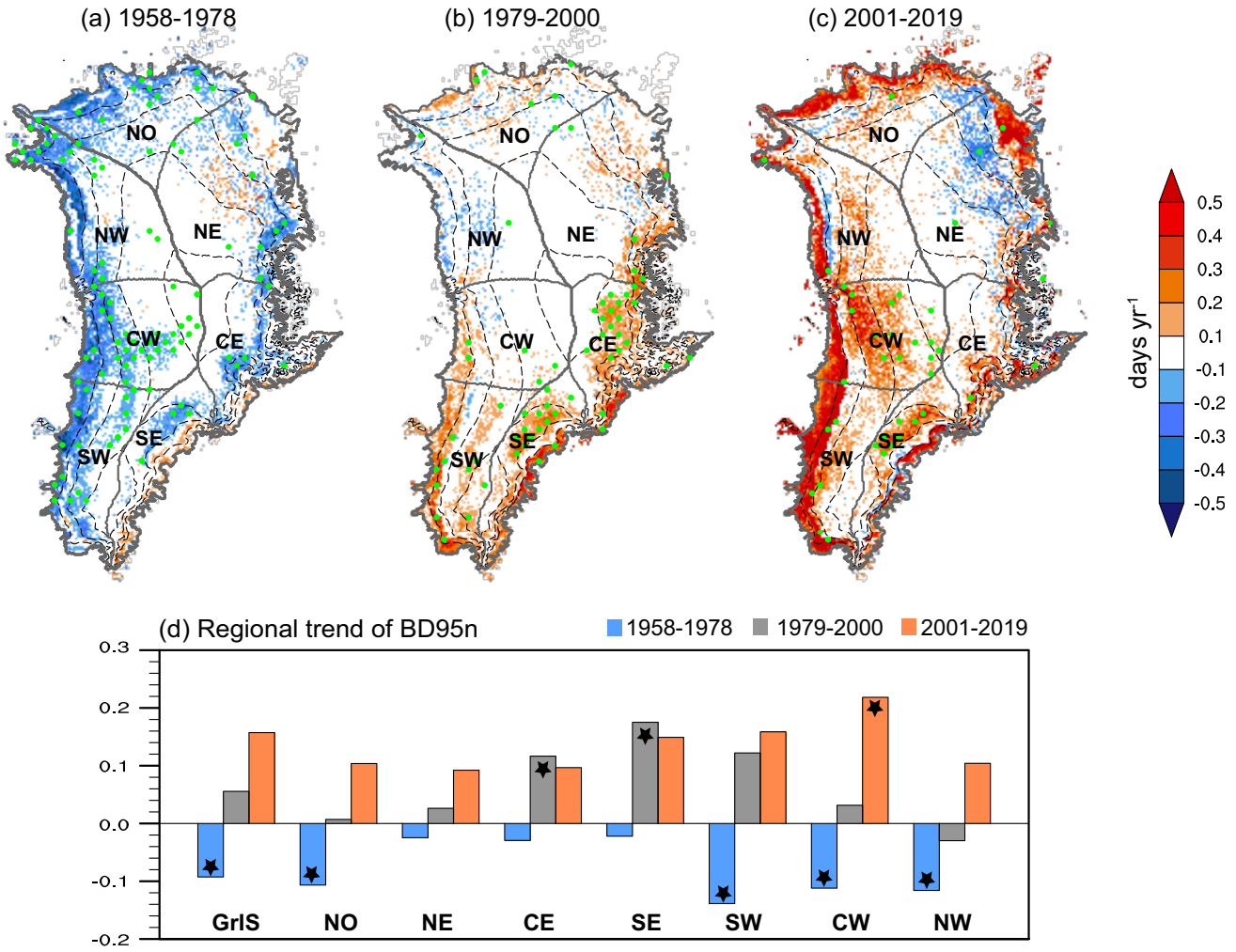

FIGURE 5 (a–c) The distribution of annual BD95n trend during (a) P1 (1958–1978), (b) P2 (1979–2000), and (c) P3 (2001–2019) periods. (d) Regionally averaged trend in BD95n during the three subperiods. The trend that is statistically significant at 90% level is marked with green dots and stars. [Colour figure can be viewed at wileyonlinelibrary.com]

3.2 | Extreme accumulation-dominated events

3.2.1 | Intensity

Figure 6a shows the climatological distribution of the maximum daily SMB (i.e., AX) over the GrIS during 1958–2019. The pattern of annual AX is broadly consistent with the distribution of precipitation, with relatively larger value along the coasts (~15.4 mm·w.e.·day^{-1} over the regions below 1,500 m) and smaller value in the interior (~4 mm·w.e.·day^{-1} over the regions above 3,000 m). The maximum daily SMB (>30 mm·w.e.·day^{-1}) is mainly observed over the southeast GrIS, where the greatest snowfall occurs (Ettema *et al.*, 2009; Huai *et al.*, 2021). For the intensity of extreme accumulation-dominated events measured by the AD95p, it shows a different climatological distribution compared with the AX. Annual AD95p is higher in the northern part and is smaller in the southern part of the GrIS (Figure 6b). This is partially attributed to the fact that AD95p reflects the relative proportion. The relative colder climate over northern Greenland contributes to higher probability of accumulation extremes. In the temporal domain, both AX, AD95p and AA averaged over Greenland show a sustained rising trend from 1958 to 2019 (Figure 6d), but with large interannual variability. This implies an increased intensity of extreme accumulation-dominated events during 1958–2019

Next, we investigate the spatial pattern of the AX trend across the GrIS during the three subperiods (Figure 7). A significant increasing trend of AX (i.e., enhanced intensity of extreme accumulation-dominated events) is observed over Greenland from 1958 to 1978, especially over the southwest GrIS where the trend reaches ~0.37 mm·w.e.·

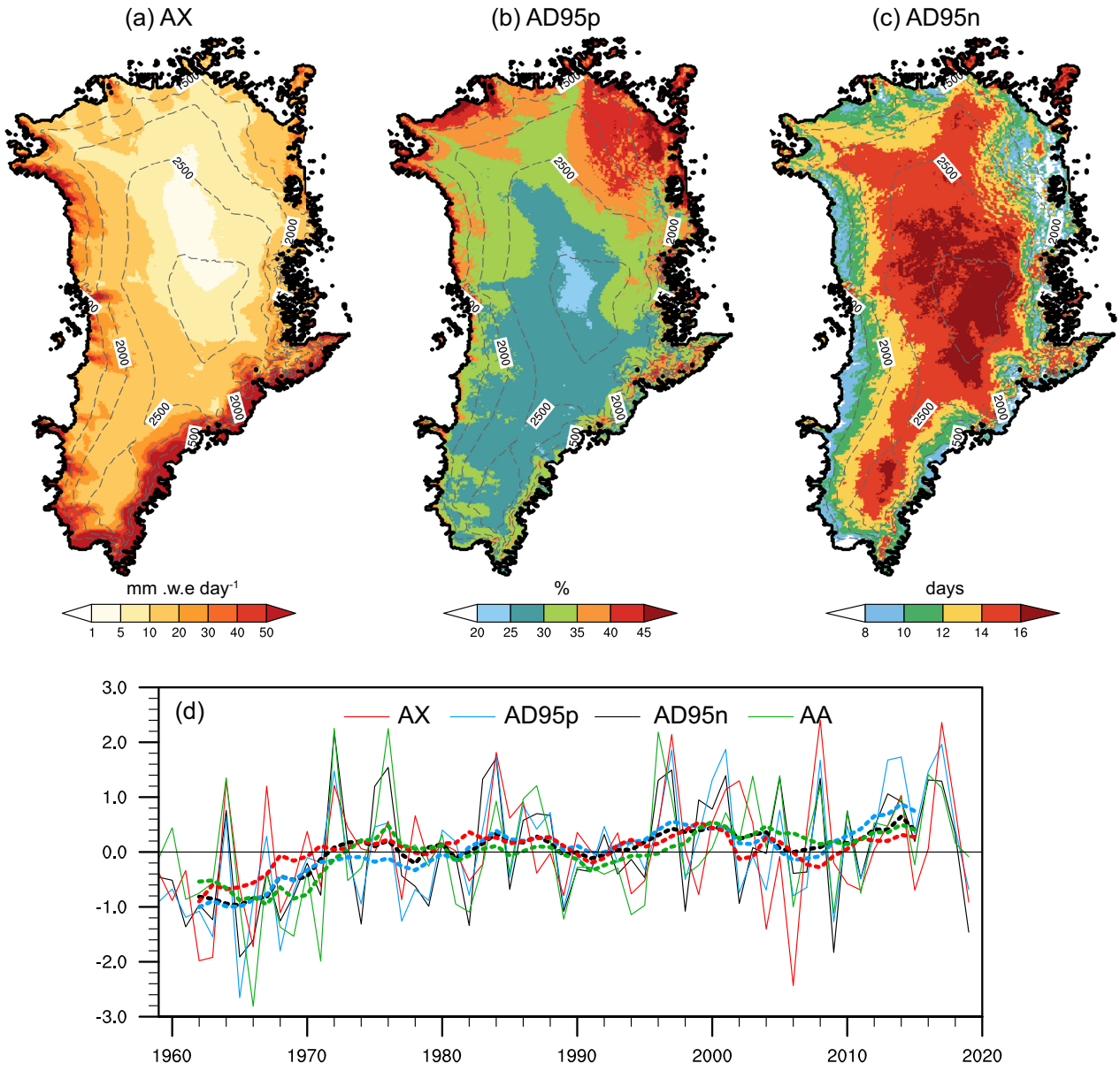

FIGURE 6 Climatological distributions of (a) AX, (b) AD95p, and (c) AD95n over the GrIS during 1958–2019. (d) The standardized time series of AX, AD95p, AD95n and AA averaged over the GrIS (solid lines) from 1958 to 2019 and its 9-year running mean (dotted lines) [Colour figure can be viewed at wileyonlinelibrary.com]

day^{-1}·year^{-1}. In contrast, the increasing trend of regionally averaged AX gets much weaker and insignificant during 1979–2000, and then turns to an opposite direction during 2001–2019, indicating a weakened intensity of extreme accumulation-dominated events. However, the trends of AX over subregions of the GrIS generally do not pass the 90% level of significance test, owing to the large spatial variability. Despite an overall similarity, the trends of AX and AA differ to some extent at regional scale in terms of sign, magnitude, and statistical significance. As shown in Figure 7, AA shows a weakening trend over southeast GrIS from 1958 to 2000 while an enhancing trend after 2000. This is the opposite to the trend in AX over there. In addition, the trend of AA over the NW and CW is also opposite to that of AX from 2000 to 2019, but the trend is not statistically significant.

The AD95p, the other indicator for the intensity of extreme accumulation-dominated events, shares some similarity with the variation of the AX, though spatial differences exist (Figure 8). Briefly, the AD95p tends to increase over the southwestern parts of Greenland (0.3%·year^{-1}) while it decreases over the northeast part during 1958–1978. This meridional dipole pattern is also seen in

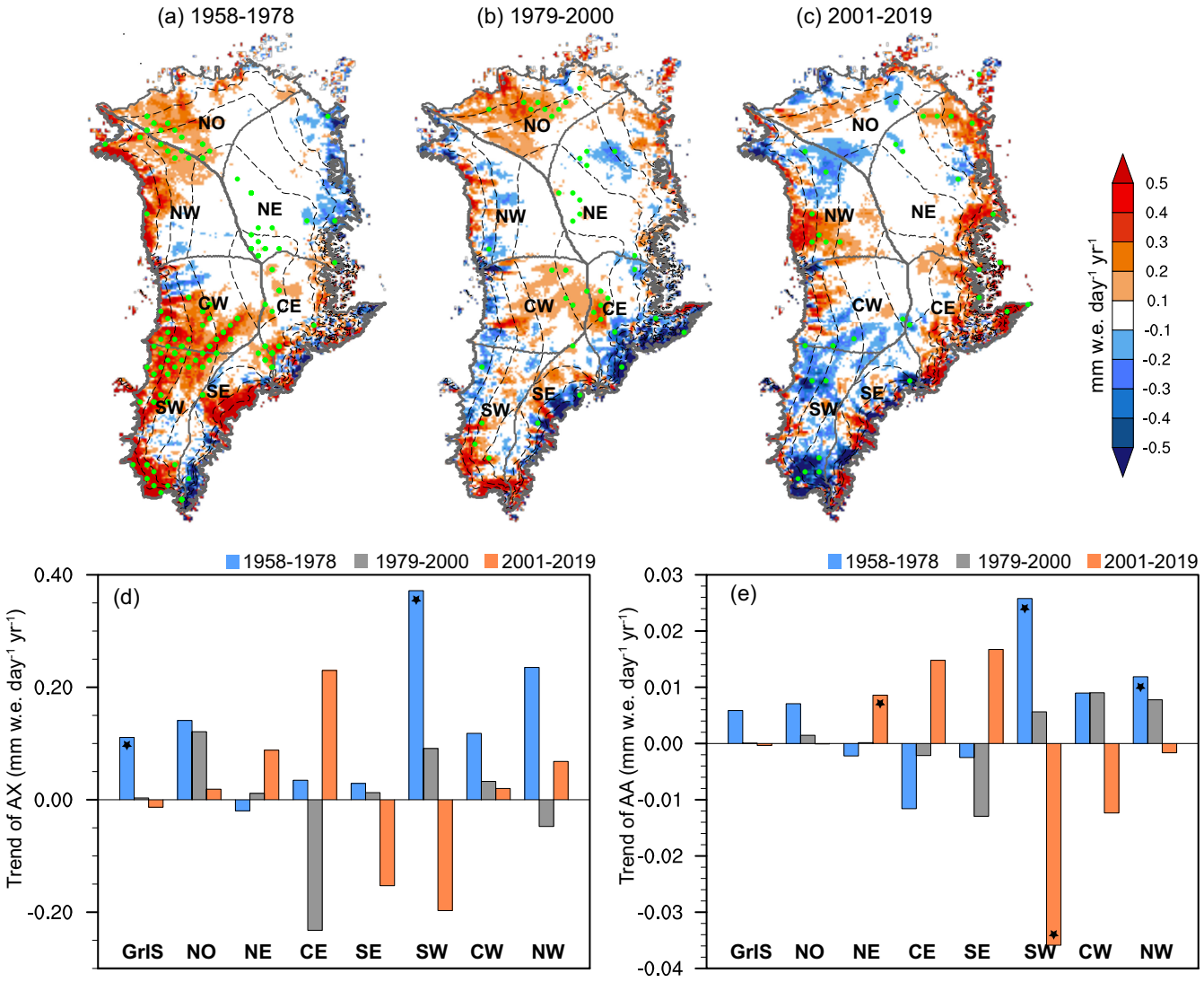

FIGURE 7 (a–c) The distribution of annual AX trend during (a) P1 (1958–1978), (b) P2 (1979–2000), and (c) P3 (2001–2019) periods. Regionally averaged trend in (d) AX and (e) AA during the three subperiods. The trend that is statistically significant at 90% level is marked with green dots and stars. [Colour figure can be viewed at wileyonlinelibrary.com]

the variation of the AX. A similar pattern broadly holds during the period of 1979–2000, though with weaker magnitude and spatial differences. In contrast, the AD95p exhibits a significant increasing trend during 2001–2019 in the northeast GrIS (0.59%·year^{-1}), while a decreasing trend is mainly observed over the southern GrIS. The accumulation zone is the region where annual snow accumulation exceeds the ablation that is largely driven by summer temperature. Annual precipitation tends to increase (decrease) over the western GrIS while decrease (increase) over the east part during 1958–1978 (2001–2019), but with no clear regional difference in summer temperature (Figure 11). Thus, the meridional dipole pattern of extreme accumulation-dominated events may be largely tied to the change in precipitation.

3.2.2 | Frequency

The frequency of extreme accumulation-dominated events shows an increasing pattern from the coastal to inland areas in terms of climatological distribution based on the AD95n (Figure 6c). This distribution is broadly opposite to the distribution of extreme ablation-dominated days (i.e., BD95n), showing a coast-to-inland increasing pattern. The annual AD95n is approximately 6–8 days averaged over the marginal areas, and increases to ~16–18 days for elevations >3,000 m.

With respect to the temporal evolution, annual AD95n shows an increasing trend during 1958–1978, but with obvious spatial differences (Figure 9). A significant increasing trend is mainly observed over the southwest (0.27 days·year^{-1}) and northwest (0.21 days·year^{-1}) GrIS,

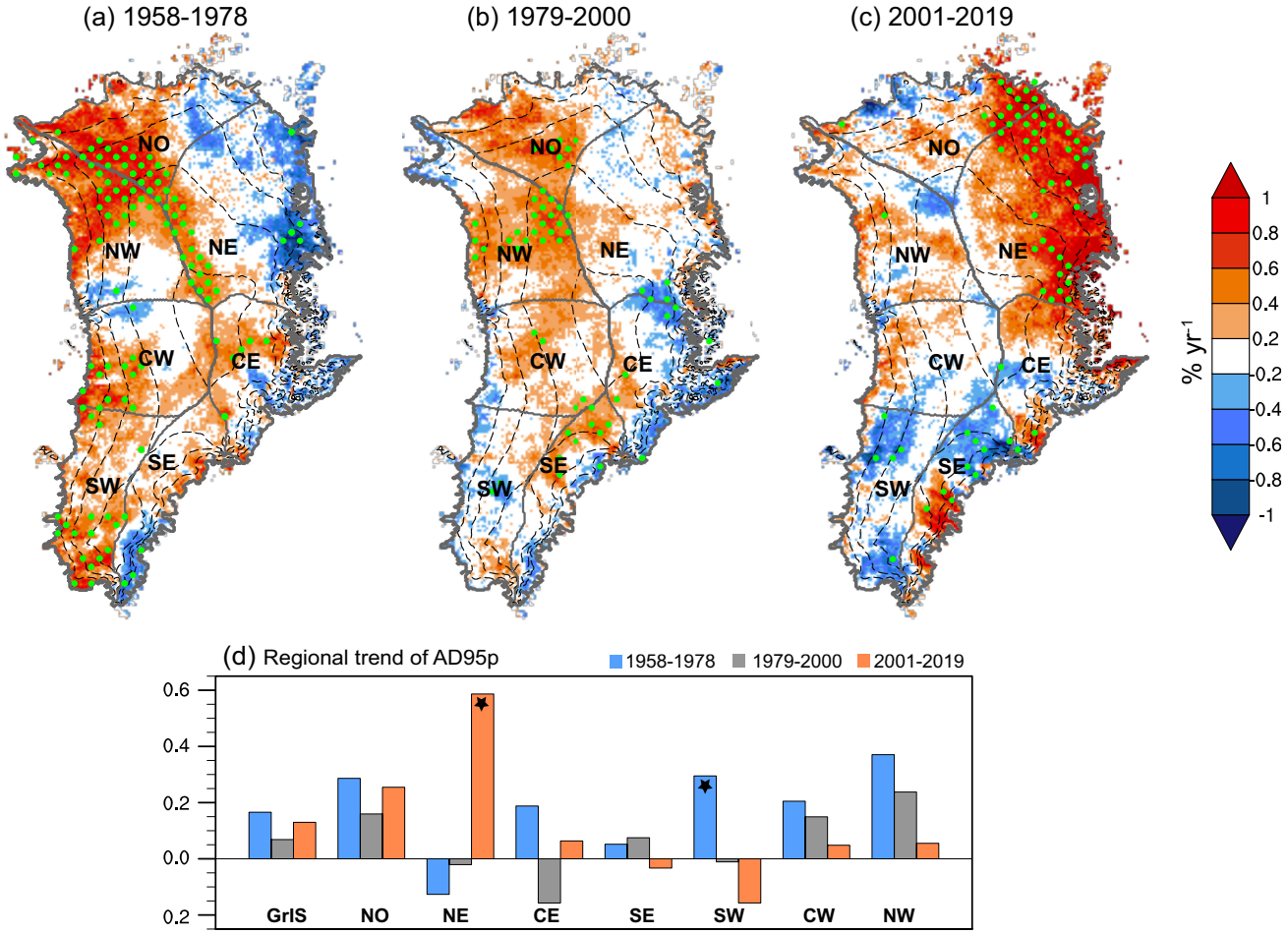

FIGURE 8 (a–c) The distribution of annual AD95p trend during (a) P1 (1958–1978), (b) P2 (1979–2000), and (c) P3 (2001–2019) periods. (d) Regionally averaged trend in AD95p during the three subperiods. The trend that is statistically significant at 90% level is marked with green dots and stars [Colour figure can be viewed at wileyonlinelibrary.com]

highlighting more frequent extreme accumulation-dominated events over the two regions. However, the AD95n shows an insignificant decreasing trend over the northeast GrIS from 1958 to 1978. During the period of 1979–2000, the AD95n also shows an increasing trend but only passing the significance test over the northwest GrIS (0.22 days·year^{-1}). From 2001 to 2019, there is no significant change in extreme accumulation-dominated days averaged over the GrIS. This is largely attributed to the offsets between the decreasing trend (−0.2 days·year^{-1}) over the southwest GrIS and the increasing trend (0.32 days·year^{-1}) over the northeast GrIS.

3.3 | Large-scale climatic background for the variations of SMB extremes

SMB represents the difference between mass gain mainly from snowfall and mass loss mainly from meltwater runoff, which is hence strongly tied to regional temperature and precipitation changes. Therefore, we first attempt to examine the linkage between change in mean SMB and temperature/precipitation. Figure 10 shows the evolution of SMB, precipitation and temperature averaged over Greenland in boreal summer from 1958 to 2019. Before 1978, summer precipitation averaged over Greenland showed a significant increasing trend (0.026 mm·day^{-1}·year^{-1}, passing the 99% level of significance test), while there was no significant change in summer temperature. Therefore, the increase of precipitation seems to play a major role in the increasing summer SMB during 1958–1978, though the variations of precipitation and temperature may be interconnected. After 1978, Greenland's summer temperature warmed rapidly (0.036°C·year^{-1}), accompanied by a decline in precipitation (−0.007 mm·day^{-1}·year^{-1}), contributing to the continuous decline in summer SMB.

Next, we further study spatial patterns of temperature/precipitation trend and the associated atmospheric

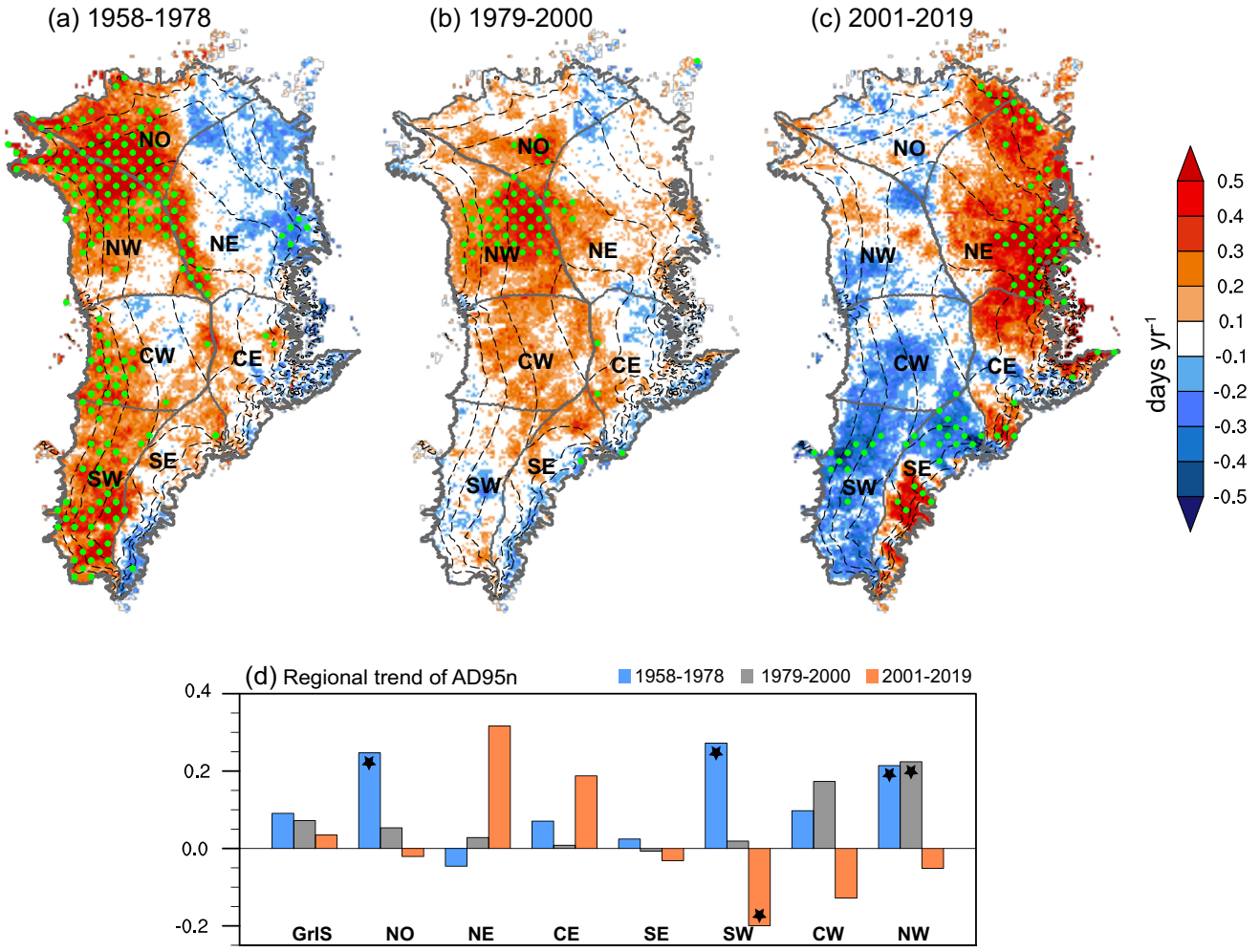

FIGURE 9 (a–c) The distribution of annual AD95n trend during (a) P1 (1958–1978), (b) P2 (1979–2000), and (c) P3 (2001–2019) periods. (d) Regionally averaged trend in AD95n during the three subperiods. The trend that is statistically significant at 90% level is marked with green dots and stars [Colour figure can be viewed at wileyonlinelibrary.com]

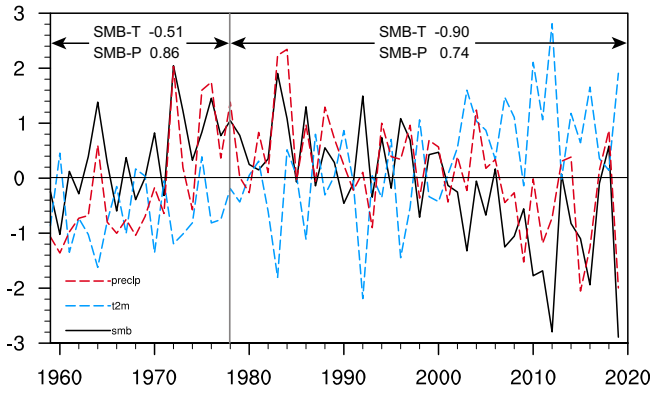

FIGURE 10 The standard time series of summer temperature, precipitation and SMB averaged over the GrIS (solid lines) and their correlation coefficients [Colour figure can be viewed at wileyonlinelibrary.com]

circulations to explore their influences on the variations of SMB extremes. As shown in Figure 11, atmospheric circulations experience significant changes around the late-1970s and early-2000s. During 1958–1978, a decreasing trend of summer geopotential height at 500 hPa (Z500) over Greenland indicates a reduced Greenland blocking (Figure 11a), which is a climatological high-pressure blocking across the entire Greenland and has been proven to be correlated with the GrIS melting events (Fettweis *et al.*, 2013; McLeod and Mote, 2015; Hanna *et al.*, 2021). The weakened blocking flow tends to enhance the circumpolar westerlies that transport warm, moist air from the North Atlantic Ocean into Greenland, leading to more precipitation over the southern and western Greenland (Figure 11d) that favours accumulation. Meanwhile, the southwestern low-lying region experiences a remarkable summer cooling that hampers ablation, although central Greenland experiences a warming (Figure 11g). Therefore, the wetter condition in tandem with regional cooling contributes to the increase/decrease in summer extreme accumulation/ablation-dominated events over

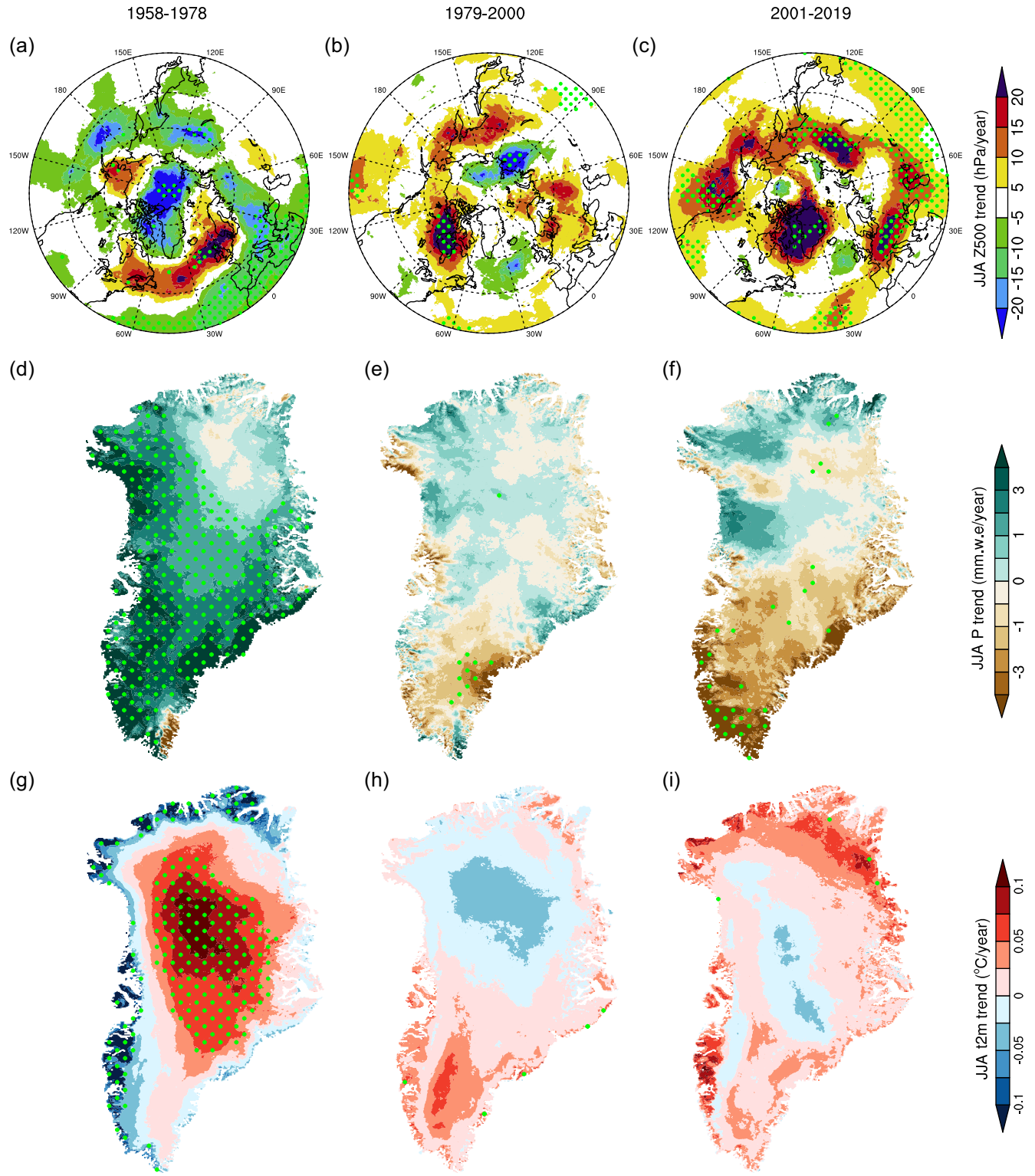

FIGURE 11 The linear trend of (a–c) geopotential height at 500 hPa (Z500), (d–f) air temperature and (g–i) precipitation during the period of 1958–1978, 1979–2000 and 2001–2019. The trend that is statistically significant at 90% level is marked with dotted area. The geopotential height and wind vector datasets in the figure come from ERA5. Temperature and precipitation data come from the simulation of RACMO2.3p2 [Colour figure can be viewed at wileyonlinelibrary.com]

the southwestern Greenland, where the most significant changes in extreme events are observed (e.g., Figures 3a and 6a).

Moreover, an obvious transition from the P1 to P2 period is observed, with a reverse of the trend in atmospheric circulations (Figure 11b). The southern

Greenland is controlled by the dry northeasterly winds during 1979–2000, leading to decreased precipitation (Figure 11e) and hence contributing to the decreasing extreme accumulation-dominated events over there. Meanwhile, Greenland experiences a remarkable warming in the southern part but cooling in the northern part (Figure 11h). The regional warming is favourable for the occurrence of extreme ablation-dominated events over the southern Greenland (e.g., Figures 3b and 4b).

The climatic conditions during the period 2001–2019 show a similar pattern in trend relative to the period 1979–2000, but with larger amplitude. It has been suggested that the GrIS on average has experienced an accelerated warming since 2000s that triggers the significant decrease in SMB (e.g., Fettweis *et al.*, 2013; Noël *et al.*, 2019). However, the warming is not uniform across Greenland during 2001–2019 (Figure 11i). Summer temperature in the northern and southern Greenland shows a warming trend, while it is slightly cooling over the interior (>2,500 m). The warming provides a favourable background for the increase/decrease in extreme ablation/accumulation-dominated events over the southern Greenland. Meanwhile, the persistent high-pressure anomaly over Greenland (Figure 11c) results in reduced cloudiness, which induces increased runoff in the southwest GrIS through enhanced absorption of solar radiation (Noël *et al.*, 2019), contributing to the increased extreme ablation-dominated events in the southwest Greenland (e.g., Figure 5c). Moreover, the high-pressure anomaly indicates an intensified blocking, which enhances southeasterly winds and leads to decreased precipitation in the southern Greenland (Figure 11f) (Pfahl and Wernli, 2012; Schaller *et al.*, 2018). The decreased precipitation contributes to the increase/decrease in extreme ablation/accumulation-dominated events in that region (e.g., Figures 5c and 11c). Notably, the dominating factor of circulations may vary with different extreme indices and time intervals. Therefore, the evolution of SMB extremes and the underlying mechanisms require further investigation.

4 | CONCLUSIONS

In this study, we develop a suite of indices for SMB extremes over Greenland and investigate their spatiotemporal variations during 1958–2019 based on RACMO2.3p2 model. In terms of climatological distribution, the intensity (BX and BD95p) and frequency (BD95n) of extreme ablation-dominated events broadly decrease from coastal to inland Greenland, consistent with the distribution of mean SMB. The intensity of extreme accumulation-dominated events measured by AX also show a coastal-to-inland decreasing pattern, but the intensity as indicated by AD95p shows a northern-to-southern decreasing pattern. In contrast, a reverse pattern (i.e., increasing from the coast to inland) is observed in frequency of the extreme accumulation-dominated events (AD95n).

Regarding the temporal trend, there is a decreasing trend over the GrIS during 1958–1978 for the intensity and frequency of extreme ablation-dominated events. The declining trend is more profound over the southwest and north GrIS, where the trend reaches −0.42 to −0.49%·year^{-1} for the intensity and −0.11 to −0.14 days·year^{-1} for the frequency. During 1979–2000, the intensity of extreme ablation-dominated events shows an increasing trend over the majority of the GrIS, especially over the central-west and southern parts of Greenland (0.36–0.45%·year^{-1}). Meanwhile, the frequency of extreme ablation-dominated events increases significantly over the central-east and southeast GrIS (0.12–0.18 days·year^{-1}). From 2001 to 2019, the extreme ablation-dominated events tend to be stronger and more frequent over GrIS relative to the previous period, especially in the central-west part, where the trend reaches 0.42%·year^{-1} for the intensity and 0.22 days·year^{-1} for the frequency.

In contrast, the extreme accumulation-dominated events experience, on average, a long-term increasing trend from 1958 to 2019 in terms of both intensity and frequency. However, obvious spatial discrepancies exist across the GrIS, especially between the southwest and northeast GrIS where an opposite trend is obviously observed during 1958–1978 and 2001–2019. During 1958–1978, enhanced (0.3%·year^{-1}) and more frequent (0.27 mm·w.e.·day^{-1}·year^{-1}) extreme accumulation-dominated events are found over the southwest GrIS, but with an insignificant decrease in intensity and frequency over the northeast GrIS. A similar pattern broadly holds between 1979 and 2000, though with a weaker magnitude. From 2001 to 2019, an opposite pattern is observed that the extreme accumulation-dominated events exhibit a significant increasing trend in the northeast GrIS (0.32 days·year^{-1} for the frequency) but a decreasing trend in the southwest GrIS (−0.2 days·year^{-1} for the frequency).

The variations of SMB extremes are linked with the changes in regional temperature/precipitation and the associated atmospheric circulations. Regarding the southwest GrIS where the most significant change is observed, the increasing precipitation due to the intensified circumpolar westerlies as well as regional cooling contribute to the decrease (increase) of extreme ablation (accumulation)-dominated events during the period of 1958–1979. Afterwards, especially in the recent two decades (2001–2019), opposite anomalous circulation pattern results in reduced cloudiness and precipitation, in tandem with remarkable regional warming. These conditions lead to the increase (decrease) of extreme ablation

(accumulation)-dominated events over the southern GrIS. Notably, the relationship between SMB extremes and large-scale circulations is more complex than the mean SMB, and the dominating factor may vary with different extreme indices and time intervals. Therefore, the evolution of SMB extremes and the underlying mechanisms require further investigation. Given the scarce of long-time observations for daily SMB, it is difficult to constrain the model results directly. The quantitative results reported here may be dependent to some extent on the global climatic forcing and the regional climate model used. However, the qualitative results (e.g., accelerated increase in BX during 2001–2019) should be largely unchanged, as summer temperature and precipitation over Greenland shows a similar trend among different reanalysis datasets. Although it is out of the scope of the current study, the sensitivity of the modelled extreme SMB events to numerical model and external forcings is worth of further investigation in future.

In this study, we for the first time develop a series of extreme indices to measure the intensity and frequency of extreme events in SMB over the GrIS, and present their spatiotemporal evolution from 1958 to 2019 based on RACMO2.3p2 model. Our results may advance our understanding of the GrIS SMB variability and help to comprehensively assess the effect of climate change on the Greenland cryosphere and ecosystems. Additionally, the features of these SMB extremes may contribute to the design of future Greenland observational networks.

ACKNOWLEDGEMENTS

This study was funded by the National Natural Science Foundation of China (41975120) and the Strategic Priority Research Program of the Chinese Academy of Sciences (XDA2010030807). Brice Noël was funded by the NWO VENI grant VI.Veni.192.019.

AUTHOR CONTRIBUTIONS

Ting Wei: Conceptualization; investigation; methodology; writing – original draft. **Brice Noël:** Data curation; methodology; software; writing – review and editing. **Minghu Ding:** Investigation; methodology; writing – review and editing. **Qing Yan:** Conceptualization; methodology; writing – review and editing.

ORCID

Ting Wei https://orcid.org/0000-0001-9822-6494

REFERENCES

AMAP. (2021) *Arctic Climate Change Update 2021: Key Trends and Impacts. Summary for Policy-makers*. Tromsø: Arctic Monitoring and Assessment Programme (AMAP), 16 pp.

Box, J.E., Fettweis, X., Stroeve, J.C., Tedesco, M., Hall, D.K. and Steffen, K. (2012) Greenland ice sheet albedo feedback: thermodynamics and atmospheric drivers. *Cryosphere*, 6, 821–839.

Cohen, J., Screen, J., Furtado, J.C., Barlow, M., Whittleston, D., Coumou, D., Francis, J., Dethloff, K, Entekhabi, D., Overland, J. and Jones, J. (2014) Recent Arctic amplification and extreme mid-latitude weather. *Nature Geoscience*, 7, 627–637.

Edwards, T.L., Fettweis, X., Gagliardini, O., Gillet-Chaulet, F., Goelzer, H., Gregory, J.M., Hoffman, M., Huybrechts, P., Payne, A.J., Perego, M., Price, S., Quiquet, A. and Ritz, C. (2014) Effect of uncertainty in surface mass balance–elevation feedback on projections of the future sea level contribution of the Greenland ice sheet. *Cryosphere*, 8, 195–208.

Ettema, J., van den Broeke, M.R., van Meijgaard, E., van de Berg, W.J., Bamber, J.L., Box, J.E. and Bales, R.C. (2009) Higher surface mass balance of the Greenland ice sheet revealed by high resolution climate modeling. *Geophysical Research Letters*, 36, L12501.

Fettweis, X., Hanna, E., Lang, C., Belleflamme, A., Erpicum, M. and Gallée, H. (2013) Brief communication "Important role of the mid-tropospheric atmospheric circulation in the recent surface melt increase over the Greenland ice sheet". *Cryosphere*, 7, 241–248.

Fettweis, X., Hofer, S., Krebs-Kanzow, U., Amory, C., Aoki, T., Berends, C.J., Born, A., Box, J.E., Delhasse, A., Fujita, K., Gierz, P., Goelzer, H., Hanna, E., Hashimoto, A., Huybrechts, P., Kapsch, M.-L., King, M.D., Kittel, C., Lang, C., Langen, P.L., Lenaerts, J.T.M., Liston, G.E., Lohmann, G., Mernild, S.H., Mikolajewicz, U., Modali, K., Mottram, R.H., Niwano, M., Noël, B., Ryan, J.C., Smith, A., Streffing, J., Tedesco, M., van de Berg, W.J., van den Broeke, M., van de Wal, R.S.W., van Kampenhout, L., Wilton, D., Wouters, B., Ziemen, F. and Zolles, T. (2020) GrSMBMIP: intercomparison of the modelled 1980–2012 surface mass balance over the Greenland ice sheet. *Cryosphere*, 14, 3935–3958.

Frederikse, T., Landerer, F., Caron, L., Adhikari, S., Parkes, D., Humphrey, V.W., Dangendorf, S., Hogarth, P., Zanna, L., Cheng, L. and Wu, Y.H. (2020) The causes of sea-level rise since 1900. *Nature*, 584, 393–397.

Golledge, N.R., Keller, E.D., Gomez, N., Naughten, K.A., Bernales, J., Trusel, L.D. and Edwards, T.L. (2019) Global environmental consequences of twenty-first-century ice-sheet melt. *Nature*, 566(7742), 65–72.

Graham, R.M., Cohen, L., Petty, A.A., Boisvert, L.N., Rinke, A., Hudson, S.R., Nicolaus, M. and Granskog, M.A. (2017) Increasing frequency and duration of Arctic winter warming events. *Geophysical Research Letters*, 44, 6974–6983.

Hanna, E., Fettweis, X., Mernild, S.H., Cappelen, J., Ribergaard, M. H., Shuman, C.A., Steffen, K., Wood, L. and Mote, T.L. (2014) Atmospheric and oceanic climate forcing of the exceptional Greenland ice sheet surface melt in summer 2012. *International Journal of Climatology*, 34, 1022–1037.

Hanna, E., John Cappelen, J., Fettweis, X., Mernild, S.H., Mote, T.L., Mottram, R., Steffen, K., Ballinger,T.J. and Hall, R. J. (2021) Greenland surface air temperature changes from 1981 to 2019 and implications for ice-sheet melt and mass-balance change. *International Journal of Climatology*, 41(Suppl.1), E1336–E1352.

Huai, B.J., van den Broeke, M.R., Reijmer, C.H., and Cappellen, J. (2021) Quantifying rainfall in Greenland: a combined

observational and modeling approach. *Journal of Applied Meteorology and Climatology*, 60, 1171–1188. https://doi.org/10.1175/JAMC-D-20-0284.1.

Liu, Y., Hallberg, R., Sergienko, O., Samuels, B.L., Harrison, M. and Oppenheimer, M. (2018) Climate response to the meltwater runoff from Greenland ice sheet: evolving sensitivity to discharging locations. *Climate Dynamics*, 51(5), 1733–1751.

McLeod, J.T. and Mote, T.L. (2015) Assessing the role of precursor cyclones on the formation of extreme Greenland blocking episodes and their impact on summer melting across the Greenland ice sheet. *Journal of Geophysical Research: Atmospheres*, 120, 12357–12377.

Mouginot, J., Rignot, E., Bjørk, A.A., van den Broeke, M., Millan, R., Morlighem, M., Noël, B., Scheuchl, B. and Wood, M. (2019) Forty-six years of Greenland ice sheet mass balance from 1972 to 2018. *Proceedings of the National Academy of Sciences of the United States of America*, 116(19), 9239–9244.

Nghiem, S.V., Hall, D.K., Mote, T.L., Tedesco, M., Albert, M.R., Keegan, K., Shuman, C.A., DiGirolamo, N.E. and Neumann, G. (2012) The extreme melt across the Greenland ice sheet in 2012. *Geophysical Research Letters*, 39, L20502.

Niwano, M., Box, J.E., Wehrlé, A., Vandecrux, B., Colgan, W.T., and Cappelen, J. (2021) Rainfall on the Greenland ice sheet: present-day climatology from a high-resolution non-hydrostatic polar regional climate model. *Geophysical Research Letters*, 48, e2021GL092942.

Noël, B., van de Berg, W.J., van Wessem, J.M., van Meijgaard, E., van As, D., Lenaerts, J.T.M., Lhermitte, S., Kuipers, M.P., Smeets, C.J.P.P., van Ulft, L.H., van de RSW, W. and van den Broeke, M.R. (2018) Modelling the climate and surface mass balance of polar ice sheets using RACMO2—part 1: Greenland (1958–2016). *Cryosphere*, 12, 811–831.

Noël, B., van de Berg, W.J., Lhermitte, S., and vanden Broeke, M.R. (2019) Rapid ablation zone expansion amplifies north Greenland mass loss. *Science Advances*, 5(9), eaaw0123.

Pfahl, S. and Wernli, H. (2012) Quantifying the relevance of cyclones for precipitation extremes. *Journal of Climate*, 25, 6770–6780.

Ryan, J.C., Smith, L.C., Van As, D., Cooley, S.W., Cooper, M.G., Pitcher, L.H., and Hubbard, A. (2019) Greenland ice sheet surface melt amplified by snowline migration and bare ice exposure. *Science Advances*, 5(3), eaav3738.

Schaller, N., Sillmann, J., Anstey, J., Fischer, E.M., Grams, C.M., and Russo, S. (2018) Influence of blocking on northern European and Western Russian heatwaves in large climate model ensembles. *Environmental Research Letters*, 13(5), 054015.

Serreze, M. and Barry, R. (2011) Processes and impacts of Arctic Amplification. *Global and Planetary Change*, 77(1–2), 85–96.

Slater, T., Shepherd, A., McMillan, M., Leeson, A., Gilbert, L., Muir, A., Munneke, P., Noel, B., Fettweis, X., van den Broeke, M., and Briggs, K. (2021). Increased variability in Greenland Ice Sheet runoff from satellite observations. *Nature Communications* 12, 6069.

Tedesco, M. and Fettweis, X. (2020) Unprecedented atmospheric conditions (1948–2019) drive the 2019 exceptional melting season over the Greenland ice sheet. *Cryosphere*, 14, 1209–1223.

The IMBIE Team. (2020) Mass balance of the Greenland ice sheet from 1992 to 2018. *Nature*, 579, 233–239.

Thompson, D.W.J. and Wallace, J.M. (1998) The Arctic Oscillation signature in the wintertime geopotential height and temperature fields. *Geophysical Research Letters*, 25, 1297–1300.

Van Dalum, C.T., van de Berg, W.J. and van den Broeke, M.R. (2021) Impact of updated radiative transfer scheme in snow and ice in RACMO2.3p3 on the surface mass and energy budget of the Greenland ice sheet. *Cryopshere*, 15, 1823–1844.

Van den Broeke, M.R., Bamber, J., Ettema, J., Rignot, E., Schrama, E., van de Berg, W.J., van Meijgaard, E., Velicogna, I., and Wouters, B. (2009) Partitioning recent Greenland mass loss. *Science*, 326, 984–986.

Van den Broeke, M.R., Box, J., Fettweis, X., Hanna, E., Noël, B., Tedesco, M., van As, D., Jan van de Berg, W., and van Kampenhout, L. (2017) Greenland ice sheet surface mass loss: recent developments in observation and modeling. *Current Climate Change Reports*, 3, 345–356.

van Dalum, C. T., van de Berg, W. J., and van den Broeke, M. R. (2021). Impact of updated radiative transfer scheme in snow and ice in RACMO2.3p3 on the surface mass and energy budget of the Greenland ice sheet. *The Cryosphere*, 15, 1823–1844, https://doi.org/10.5194/tc-15-1823-2021.

How to cite this article: Wei, T., Noël, B., Ding, M., & Yan, Q. (2022). Spatiotemporal variations of extreme events in surface mass balance over Greenland during 1958–2019. *International Journal of Climatology*, *42*(15), 8008–8023. https://doi.org/10.1002/joc.7689